# $Ca^{2+}$-dependent inactivation of $Ca_v1.2$ channels prevents $Gd^{3+}$ block: does $Ca^{2+}$ block the pore of inactivated channels?


**Olga Babich**
Department of Pharmacology and Physiology,
UMDNJ - New Jersey Medical School
Newark, NJ 07103

**Victor Matveev**
Department of Mathematical Sciences
New Jersey Institute of Technology
(973)596-5619, matveev@njit.edu

**Andrew L. Harris**
Department of Pharmacology and Physiology,
UMDNJ - New Jersey Medical School
Newark, NJ 07103

**Roman Shirokov**
Department of Pharmacology and Physiology,
UMDNJ - New Jersey Medical School
Newark, NJ 07103
(973)972-8869, roman.shirokov@umdnj.edu



**CAMS Report 0607-20, Fall 2006/Spring 2007**
**Center for Applied Mathematics and Statistics**

# $Ca^{2+}$-dependent inactivation of $Ca_V1.2$ channels prevents $Gd^{3+}$ block: does $Ca^{2+}$ block the pore of inactivated channels?

Olga Babich[1], Victor Matveev[2], Andrew L. Harris[1] and Roman Shirokov[1]

[1]Department of Pharmacology and Physiology,
University of Medicine and Dentistry of New Jersey, New Jersey Medical School,
Newark, NJ 07103, USA;
[2]Department of Mathematical Sciences,
New Jersey Institute of Technology,
Newark, NJ 07102, USA.

Running title*:* Permeation and inactivation of $Ca^{2+}$ channels.

Please address correspondence to Roman Shirokov,
Department of Pharmacology and Physiology,
UMDNJ, New Jersey Medical School,
185 South Orange Avenue,
Newark, NJ 07103.

Telephone: (973) 972 8869
Fax: (973) 972 7950
E-mail: roman.shirokov@umdnj.edu

March 2007

## Abstract

Lanthanide gadolinium ($Gd^{3+}$) blocks $Ca_V1.2$ channels at the selectivity filter. Here we investigated whether $Gd^{3+}$ block interferes with $Ca^{2+}$-dependent inactivation, which requires $Ca^{2+}$ entry through the same site. Using brief pulses to 200 mV that relieve $Gd^{3+}$ block but not inactivation, we monitored how the proportions of open and open-blocked channels change during inactivation. We found that blocked channels inactivate much less. This is expected for $Gd^{3+}$ block of the $Ca^{2+}$ influx that enhances inactivation. However, we also found that the extent of $Gd^{3+}$ block did not change when inactivation was reduced by abolition of $Ca^{2+}$/calmodulin interaction, showing that $Gd^{3+}$ does not block the inactivated channel. Thus, $Gd^{3+}$ block and inactivation are mutually exclusive, suggesting action at a common site. These observations suggest that inactivation causes a change at the selectivity filter that either hides the $Gd^{3+}$ site, or reduces its affinity, or that $Ca^{2+}$ occupies the binding site at the selectivity filter in inactivated channels. The latter possibility is supported by previous findings that the EEQE mutation of the selectivity EEEE locus is void of $Ca^{2+}$-dependent inactivation (Zong Z.Q., J.Y. Zhou, and T. Tanabe. 1994. *Biochem Biophys Res. Commun.* 201(3):1117-11123), and that $Ca^{2+}$-inactivated channels conduct $Na^+$ when $Ca^{2+}$ is removed from the extracellular medium (Babich O., D. Isaev, and R. Shirokov. 2005. *J. Physiol.* 565.3;709-717). Based on these results, we propose that inactivation increases affinity of the selectivity filter for $Ca^{2+}$ so that $Ca^{2+}$ ion blocks the pore. A minimal model, in which the inactivation "gate" is an increase in affinity of the selectivity filter for permeating ions, successfully simulates the characteristic U-shaped voltage dependence of inactivation in $Ca^{2+}$.

**Key words:** gating; selectivity; dihydropyridine; calmodulin.

## Introduction

In $Ca_V1.2$ channels, $Ca^{2+}$ selectivity and block by various polyvalent metal ions are mediated by carboxyl side chains of the four glutamates (EEEE locus) that form ion-binding site(s) (for review: Sather and McCleskey, 2003). A somewhat overlooked observation that a glutamate to glutamine substitution in the S5-S6 loop of the third repeat (EEEE to EEQE modification) eliminates $Ca^{2+}$-dependent inactivation (Zong et al., 1994) strongly indicated that the selectivity locus plays an important role in $Ca^{2+}$-dependent inactivation. Previously, we showed that $Ca^{2+}$-dependent inactivation of $Ca_V1.2$ channels specifically prevents permeation of $Ca^{2+}$, but not alkali metal ions (Babich et al., 2005). We concluded that $Ca^{2+}$-dependent inactivation controls $Ca^{2+}$ conductance by affecting the selectivity mechanism rather than by occluding the pore at a cytoplasmic inactivation gate. This leads to the idea that perhaps the selectivity filter is the gate of $Ca^{2+}$-dependent inactivation and that $Ca^{2+}$-dependent inactivation specifically prevents $Ca^{2+}$ permeation by stabilizing a high $Ca^{2+}$ affinity state of the selectivity filter.

To test this hypothesis, we analyzed how blockage of the channel by lanthanide gadolinium ($Gd^{3+}$) depends on inactivation and vice versa. This approach eliminates problems that can occur when $Ca^{2+}$ affinity of inactivated channels is assessed by simple manipulations of extracellular $Ca^{2+}$, as this by itself might change the affinity of the selectivity filter.

Like many other trivalent metal ions, $Gd^{3+}$ is a potent blocker of $Ca^{2+}$ channels. At concentrations of 10-100 nM, it reduces the peak and accelerates decay of ionic current during depolarization. This accelerated decay has been proposed to be due to an

increase of the potency of block of open rather than closed channels (Biagi and Enyeart, 1990; Obejero-Paz, 2004), or because trivalent metal ions accelerate inactivation by acting at a site that is different from the blocking site (Beedle et al., 2002).

The results of the accompanying paper (Babich et al., 2007) explain the voltage-dependent enhancement of $Gd^{3+}$ block by linking it to activation directly, rather than via inactivation. Similarly, inactivation also increases with voltage because it is also linked to activation. In addition, $Gd^{3+}$ block is relieved at high positive voltages, generating a characteristic U-shaped dependence on voltage. The complex voltage-dependence of $Gd^{3+}$ block is very similar to that of $Ca^{2+}$-dependent inactivation, which parallels $Ca^{2+}$ influx rather than voltage (Brehm & Eckert, 1978). This makes it tempting to suggest that $Gd^{3+}$ binding stabilizes channels in an inactivated state, similar to the action of other $Ca^{2+}$ channel blockers (e.g., dihydropyridines). However, we (Babich et al., 2007) showed that the U-shaped voltage-dependence of $Gd^{3+}$ block is not affected by tampering with regulation of inactivation by calmodulin (Lee et al., 1999; Peterson et al., 1999; Qin et al., 1999; Zuhlke et al., 1999). The results presented below demonstrate that $Gd^{3+}$ block actually reduces $Ca^{2+}$-dependent inactivation. Moreover, the reverse is also true: $Ca^{2+}$ inactivation reduces $Gd^{3+}$ block. Thus, although inactivation is not a prerequisite of the U-shaped voltage-dependence of $Gd^{3+}$ block, both inactivation and $Gd^{3+}$ block are linked to activation and depend on electro-diffusion into the pore in a similar fashion.

Since $Gd^{3+}$ block is strongly influenced by permeant ions, we suggest that $Ca^{2+}$-dependent inactivation reduces $Gd^{3+}$ binding by increasing the occupancy of the binding

site by permeant ion(s). Based on our findings, we developed a model that successfully describes the U-shaped voltage-dependence of $Ca^{2+}$-dependent inactivation as a result of an increase of the affinity of the selectivity filter to $Ca^{2+}$. This view does not contradict the effects of $Ca^{2+}$/calmodulin on inactivation of these channels, but rather places the mechanistic focus of the permeability changes at the selectivity filter.

## Methods

Channel expression and patch-clamp technique were as described in the accompanying paper (Babich et al., 2007).

### Online Supplemental Material.

The additional material (available at http://www.jgp.org) contains script text files that were used to run the simulations described in the text. The file cain.par contains the equations, parameters of the model, and extensive comments. The file cain2.par is a modification of cain.par to model the effect of $Ca^{2+}$ accumulation. The calculation program CalC for the scripts is available at http://web.njit.edu/~matveev/. Supplemental Fig. 1S illustrates simulation of the dependence of inactivation kinetics on series resistance. Supplemental Fig. 2S illustrates simulation of the dependence of inactivation kinetics on single-channel current. Supplemental Fig. 3S illustrates simulation of inactivation in $Ba^{2+}$.

## Results

### *$Gd^{3+}$ block prevents $Ca^{2+}$-dependent inactivation.*

Although both inactivation and blockage reduce ionic currents, it is possible to evaluate their specific contributions using pulse protocols that exploit the removal of $Gd^{3+}$ block at large positive voltages. Thus, we used a 20 ms pulse to 200 mV to unblock $Gd^{3+}$ during development of both inactivation and $Gd^{3+}$ block. The pulse to 200 mV was applied at different times during a much longer voltage pulse to 20 mV that activated maximal $Ca^{2+}$ currents (Fig. 1A). In the absence of $Gd^{3+}$ (Fig. 1B), the peaks of tail currents after the pulses to 200 mV reflected the onset of inactivation that occurred during the step from the holding potential to 20 mV before the pulses to 200 mV were applied. The peaks were somewhat larger than the current just before the pulses to 200 mV were applied reflecting a small additional increase in the degree of activation between 20 and 200 mV. At 50 nM $Gd^{3+}$ (panel C), the tail currents increased in comparison with those in the absence of the blocker. Because the sub-$\mu$M amounts of $Gd^{3+}$ do not affect the voltage-dependence of activation (Babich et al., 2007), the increase was unlikely to be due an additional activation at 200 mV. Since the pulse to 200 mV removes $Gd^{3+}$ from open-blocked channels, the magnitude of tail currents in the presence of $Gd^{3+}$ reflects the number of channels that were opened and opened-blocked just before the unblocking pulse was applied. The current activated by stepping from –90 to 20 mV further decreased and decayed much more quickly when 1 $\mu$M $Gd^{3+}$ was added to the bathing solution (panel D), but the tail currents caused by stepping from 200 to 20 mV increased even more in comparison with those in panels B and C. Similar observations were seen in 6 cells. Without exception, addition of $Gd^{3+}$ reduced

currents activated by the test depolarization but increased the tail currents after the pulse to 200 mV.

The increase of the number of channels that were opened and opened-blocked (O+OB) reflected a reduction of inactivation due to the presence of $Gd^{3+}$. In principle, $Gd^{3+}$ could bind to inactivated channels as well. Thus, the extent of inactivation calculated as 1-(O+OB) reflects the number of inactivated and potentially inactivated-blocked channels. A minimal Scheme I to describe the interaction between inactivation and $Gd^{3+}$ is that of state-dependent binding of $Gd^{3+}$.

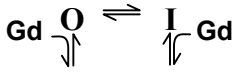

**Scheme I**

The observation that O+OB increases with [$Gd^{3+}$] indicates that inactivation is reduced in blocked states, i.e., the rate of the OB→IB transition is small and the reverse transition is not changed. This is consistent with the idea that block reduces $Ca^{2+}$ influx needed for the $Ca^{2+}$/calmodulin regulation.

***$Gd^{3+}$ block does not increase inactivation in $Ba^{2+}$.***

Experiments illustrated in Fig. 2 analyze how $Gd^{3+}$ block affects inactivation of $Ba^{2+}$ currents. The test pulse from –90 to 0 mV activated maximal $Ba^{2+}$ current. The steps from 0 to 200 mV and back to 0 mV caused tail currents, whose peaks indicate the degree of inactivation (I + IB). To avoid current run-down due to intracellular accumulation of $Ba^{2+}$ during prolonged pulses, only two sets of pulses with 5 ms and 500 ms long initial steps to 0 mV were taken in each cell. The magnitude of the tail currents (i.e., degree of inactivation) did not decrease in the presence of $Gd^{3+}$ even

though the blocker reduced and accelerated decay of currents during the pulse from –90 to 0 mV. In 3 cells tested by the same experimental protocol as on Fig. 2, the tail currents elicited by stepping from 200 to 0 mV did not change in the presence of $Gd^{3+}$. In 2 cells, addition of $Gd^{3+}$ caused a small (~10%) increase of the tails consistent with inactivation in $Ba^{2+}$ also depending to small degree on ion influx (Ferreira et al., 1997). These results show that the effects of $Gd^{3+}$ block on inactivation are more pronounced for $Ca^{2+}$, rather than $Ba^{2+}$, conductance.

***$Ca^{2+}$-dependent inactivation prevents $Gd^{3+}$ block.***

The data in Fig. 1 indicate that blocked channels do not inactivate and the distribution in the OB↔IB step of Scheme I is shifted towards the OB state. Therefore, $Gd^{3+}$ binding to the inactivated state could significantly increase the portion of open-blocked channels (I→IB→OB) in addition to the direct block (O→OB). In other words, binding of $Gd^{3+}$ to inactivated channels would increase the apparent efficiency of $Gd^{3+}$ for block of open channels as defined by the O/OB ratio. In the experiment in Fig. 3, we assessed whether the block could occur through binding of $Gd^{3+}$ to inactivated channels by using conditions in which inactivation is greatly reduced. For this purpose, we included a mutant calmodulin CAM1234 with low affinity to $Ca^{2+}$ in our expression system. The presence of CAM1234 dramatically reduces $Ca^{2+}$-dependent inactivation (Peterson et al., 1999). In Fig. 3, the pulse protocol was the same as in Fig. 1, but only traces for the 500 ms first pulse to 20 mV are shown. Despite the dramatic difference in inactivation between the wild type and the CAM1234 mutant in the absence of $Gd^{3+}$ (compare black traces), both tonic block (reduction of peak currents) and use-

dependent block (acceleration of current decay) were nearly the same (compare gray traces). This is expected since $Gd^{3+}$ prevents inactivation. Importantly, the O/OB ratio determined from the peak currents following the pulse to 200 mV was not significantly different in cells with normal or mutated calmodulin. Therefore, inactivation did not change the re-equilibration between opened and opened-blocked channels. We conclude that there is no significant occupancy of an IB state, i.e. $Gd^{3+}$ does not bind to inactivated channels.

## Discussion

***Hypothesis: $Ca^{2+}$ ions occlude the selectivity locus during $Ca^{2+}$-dependent inactivation.***

Our observations indicate that $Ca^{2+}$-dependent inactivation and $Gd^{3+}$ block of $Ca_V1.2$ channels are mutually exclusive, suggesting direct or allosteric action at a common site. A possible mechanism is that $Ca^{2+}$-dependent inactivation decreases $Gd^{3+}$ binding, and that $Gd^{3+}$ occupancy of the site blocks inactivation. The simplest form of such a mechanism is one in which inactivation increases occupancy of the $Gd^{3+}$ site by $Ca^{2+}$.

Several lines of data suggest that the selectivity filter itself is the site of interaction between $Gd^{3+}$ and $Ca^{2+}$-dependent inactivation. $Gd^{3+}$ block is thought to occur at the selectivity filter and its potency is strongly influenced by competition with permeant ions. Inactivation has been shown to reduce specifically $Ca^{2+}$ permeability, but not permeability of monovalent ions in the absence of $Ca^{2+}$ (Babich et al., 2005). Importantly, the EEQE mutation at the selectivity locus eliminates $Ca^{2+}$-dependent inactivation while allowing $Ca^{2+}$ to permeate (Zong et al., 1994).

Thus, our studies of $Gd^{3+}$ block suggest a determining role for the selectivity filter in $Ca^{2+}$-dependent inactivation of these channels, in addition to the well-established role of calmodulin in enhancing or stabilizing the inactivated state. These ideas prompted us to determine whether a minimal model of this mechanism could account for key features of inactivation.

***The minimal model of ion-dependent inactivation.***

Starting from the idea that $Ca^{2+}$-dependent inactivation stabilizes a state of the selectivity filter with higher affinity to $Ca^{2+}$, we built a minimal model of inactivation that successfully describes the U-shaped dependence of inactivation on voltage, the signature of the current-dependent mechanism. The model incorporates only very basic assumptions about gating, ion flux, and $Ca^{2+}$ binding in the pore.

The model (Fig. 4) assumes that when $Ca^{2+}$ is not in the pore, voltage-dependent inactivation obeys the four-step Charge1-Charge2 schema (Brum and Rios, 1987; Shirokov et al., 1992). The left-right transition from R (resting) to A (activated) states is the opening of the voltage-dependent gate; the down-up transition from P (primed) to I (inactivated) states is the inactivating step. $Ca^{2+}$ binding to the pore (front-back transitions) interferes with any of the four states, making it a three-particle allosteric mechanism.

The pore of non-inactivated channels is assumed to have an apparent affinity for $Ca^{2+}$ in the 10 mM range that is sufficient to provide the $10^6$ $s^{-1}$ throughput/flux rate corresponding to the observed 0.1-1 pA single-channel currents. According to our interpretation of experimental results, the affinity increases in inactivated channels. Even in inactivated states, the microscopic kinetic steps describing $Ca^{2+}$ binding are rapid in comparison with other transitions that correspond to the channel's conformational changes. Therefore, the rapid equilibration approximation is used to describe $Ca^{2+}$ binding. This simplification allows the U-shaped voltage-dependence of inactivation to be accounted for based on the fundamentals of the link between activation/inactivation and ionic flux without making specific structural assumptions

about location of the interaction.

The rapid equilibration approximation of the intra-pore ion binding has been used to describe $H^+$ blockage of $Na^+$ channels (Woodhull, 1973) and $Ca^{2+}$ blockage of the EEEE locus in the pore of cyclic nucleotide-gated channels (Seifert et al., 1999).

Because $Ca^{2+}$ -dependent inactivation does not change the voltage-dependence of the intramembrane charge movements in non-inactivated and inactivated channels (Isaev et al., 2004), $Ca^{2+}$ binding is proposed to affect inactivation steps (P↔I), but not transitions R↔A that correspond to movement of the voltage sensor. When $Ca^{2+}$ ion is in the pore, the inactivation onset rate (P→I) is increased by a factor $\gamma$ (20-100 in calculations). Because of microscopic reversibility, this is equivalent to increasing the affinity of inactivated channels to $Ca^{2+}$ by the same factor (i.e., effective $K_{D.eff.} = K_D / \gamma$ in I states).

In addition to being coupled to the states of the channel, $Ca^{2+}$ binding in channels with open voltage-dependent gate (A states) is affected by voltage directly because the site is in the permeation pathway. If the on-off rates of $Ca^{2+}$ binding to the pore are independent on the direction from/to which $Ca^{2+}$ ions move to/from the channel 0 mV, then the effect of voltage might be accounted for by using the effective dissociation constant written as:

$$K_{D.eff.} = K_D\, f(V) = K_D\, e^{\delta V/25\ mV}\, \frac{1 + e^{-V/25\ mV}}{1 + e^{(V-2E_{Ca})/25\ mV}},$$

where $\delta$ is the portion of the electric field at the $Ca^{2+}$ binding site, $E_{Ca}$ is the equilibrium potential for $Ca^{2+}$, and the voltage steepness factor 25 mV approximates RT/F at room temperature. The formula for f(V) is an extension of the Woodhull theory of voltage-

dependent block (Woodhull, 1973) for permeating ion.

Opening of the gate and low affinity of the pore correspond to the open non-inactivated channel. In the AR states $Ca^{2+}$ can move through the channel. When the gate is open, but the channel is inactivated (the AI state), $Ca^{2+}$ flux through the channel is small because the pore has higher affinity to $Ca^{2+}$. The amplitude of single-channel current through the single site was calculated as:

$$i_{s.ch.} = ([Ca^{2+}_{in}]\, k_{on}\, e^{(1-\delta)V/25\ mV} - [Ca^{2+}_{out}]\, k_{on}\, e^{-\delta V/25\ mV})(1 - P_{Ca}),$$

where $P_{Ca}$ is the probability that the site is occupied by $Ca^{2+}$. It is equal to

$P_{Ca/AP} = 1/(1 + K_D\, f(V) / [Ca^{2+}_{out}])$ in the state AP,

and to $P_{Ca/AI} = 1/(1 + ( K_D\, f(V) / \gamma ) / [Ca^{2+}_{out}])$ in the state AI.

Other constants and details of the model are described in the script file (text file cain.par in Supplemental Material) that was used to run the calculation with the CalC modeling program (Matveev et al., 2004).

Currents simulated for a set of voltage pulses applied from –100 mV are shown in Fig. 5A. They are the sums of currents through channels in non-inactivated and inactivated states. Simulated currents through inactivated states (panel 5B) are very small. The rate of inactivation (determined by fitting a sum of an exponential and a constant) was maximal (panel 5D) at voltages where peak current (panel 5C) was maximal. Therefore, the simulation demonstrates that the U-shaped voltage dependence of inactivation can arise simply from $Ca^{2+}$ binding more potently to the pore of inactivated channels and thus preventing the influx. Inactivation increases at voltages where the channels activate because the state at which $Ca^{2+}$ blocks the pore is more likely when the voltage sensor is at the cis/active position. Inactivation decreases at

more positive voltages because diffusion of $Ca^{2+}$ that stabilizes the high affinity inactivated state of the site within the pore is reduced.

In several studies, it has been shown that the maximum rate of inactivation does not seem to correspond to the peak of the ionic current (e.g., Noceti et al., 1998). Instead, the maximal rate of inactivation occurs 10-20 mV more negative than the voltage of maximal currents. Since the driving force for $Ca^{2+}$ influx increases with voltage becoming more negative, this could be taken as evidence that the accumulation of $Ca^{2+}$ on the intracellular side of the channel, rather than its diffusion into the pore and an immediate effect on gating, is critical for the U-shaped voltage dependence of inactivation. However, the kinetics of inactivation at voltages of the negative resistance slope of the current-voltage relationship are extremely sensitive to the error in voltage clamp due to finite series resistance. The model readily reproduces the negative shift of the voltage-dependence of inactivation rate by accounting for the realistic values of series resistance, membrane capacitance, and magnitudes of trans-membrane currents (supplemental Fig. 1S).

Although it is not required to explain the U-shaped voltage-dependence of inactivation, possible contribution of the "local" accumulation of $Ca^{2+}$ can be added-on to the model (supplemental Fig. 2S). In this case, the "inactivation-block coupling" factor $\gamma$ is increased proportionally to the magnitude of the single-channel current when the channel is in conductive states. This modification also describes the observation that the rate of inactivation is maximal at voltages more negative than those causing peak currents.

To test whether or not the model critically depends on how the amplitude of

single-channel current was calculated, we also used other formulations that represent two extreme cases: Ohmic (long-channel approximation) and constant field (GHK, or short-channel approximation). While these two approaches require experimentally determined scaling factors, the single-site formulation described above calculates ionic current/flux using the same $Ca^{2+}$ on-off rates that account for the interaction with inactivation. All three formulations give similar result: inactivation of simulated ionic currents has a pronounced U-shaped voltage-dependence.

***Conclusion.***

Involvement of the pore structure in the C-type/slow inactivation of voltage-gated $K^+$ and $Na^+$ channels has been well established (Lopez-Barneo et al., 1993; Baukrowitz and Yellen, 1995; Balser et al., 1996; Starkus et al., 1997; Kiss et al., 1999; Starkus et al., 2000; Loots and Isacoff, 2000; Kuo et al., 2004, see comment by Kass, 2004; Berneche and Roux, 2005). Although participation of the selectivity filter in inactivation gating was originally proposed for $Ca^{2+}$ channels (Brum *et al*., 1988; Pizarro *et al*., 1989), understanding of its mechanisms had been delayed apparently because it was thought to be a property of voltage dependent inactivation, which is much slower and therefore of a lesser physiological significance than $Ca^{2+}$-dependent inactivation. Nevertheless, some studies that analyzed mutations in the selectivity locus of $Ca^{2+}$ channels clearly showed its involvement in rapid inactivation of L-type (Yatani et al., 1994; Zong et al., 1994) and T-type (Talavera et al., 2003) channels.

The idea that during inactivation $Ca^{2+}$ blocks the channel at the selectivity filter does not contradict the view that the calmodulin tethered to the intracellular side of the

channel is an important regulator of inactivation. To explain a more rapid inactivation and a more pronounced U-shape of voltage-dependence in $Ca^{2+}$, rather than in $Ba^{2+}$, the "inactivation-block coupling" factor $\gamma$ in our minimal model of ion-dependent inactivation should be greater in $Ca^{2+}$ than in $Ba^{2+}$ (supplemental Fig. 3S). This is in agreement with our previous suggestion (Isaev et al., 2004) that $Ca^{2+}$/calmodulin controls inactivation by stabilizing the inactivated state(s) with $Ca^{2+}$ bound to the pore. However, according to our view, the U-shaped voltage-dependence of inactivation does not occur from the $Ca^{2+}$/calmodulin interaction. It results from $Ca^{2+}$ blockage of the selectivity filter, or, more specifically, the effect of voltage on $Ca^{2+}$ accessibility to it.

In the last few years, the study of $Ca^{2+}$-dependent inactivation has been driven mostly by the analysis of the role of calmodulin. Our work demonstrates that other $Ca^{2+}$ site(s) are involved as well. The mechanism that actually stops $Ca^{2+}$ influx through inactivated channels has not been identified, but our data and modeling suggest that intra-pore $Ca^{2+}$ itself is key. Our observations strongly indicate that changes in the selectivity filter play fundamental role in the block of $Ca^{2+}$ influx during $Ca^{2+}$-dependent inactivation.

Although further studies are needed to determine specifics of the molecular mechanism that alters $Ca^{2+}$ binding to the selectivity filter during activation/inactivation gating, the theory described here provides a relatively simple framework for explaining how auxiliary subunits and calmodulin fine tune ion- and voltage- dependent inactivation by directly influencing movements of the S5-pore-S6 bundles of the $\alpha 1$ subunit.

## References


Babich O., D. Isaev, and R. Shirokov. 2005. Role of extracellular $Ca^{2+}$ in gating of $Ca_V1.2$ channels. *J. Physiol.* 565.3;709-717.

Babich O., J. Reeves, and R. Shirokov. 2007. Block of $Ca_V1.2$ channels by $Gd^{3+}$ reveals pre-opening transitions in the selectivity filter. *J. Gen. Physiol.* SUBMITTED.

Balser J.R., H.B. Nuss, N. Chiamvimonvat, M.T. Perez-Garcia, E. Marban, and G.F. Tomaselli. 1996. External pore residue mediates slow inactivation in μ1 rat skeletal muscle sodium channels. *J. Physiol.* 494:431–442.

Berneche S., and B. Roux. 2005. A gate in the selectivity filter of potassium channels. *Structure* 13(4):591-600.

Baukrowitz T., and G. Yellen. 1995. Modulation of $K^+$ current by frequency and external $[K^+]$: a tale of two inactivation mechanisms. *Neuron* 15:951-960.

Beedle A.M., J. Hamid, and G.W. Zamponi. 2002. Inhibition of transiently expressed low- and high-voltage-activated calcium channels by trivalent metal cations. *J. Membr. Biol.* 187:225-238.

Biagi B.A., and J.J. Enyeart. 1990. Gadolinium blocks low- and high-threshold calcium currents in pituitary cells. *Am. J. Physiol.* 259(3 Pt 1):C515-C520.

Brehm P., and R. Eckert. 1978. Calcium entry leads to inactivation of calcium channel in Paramecium. *Science* 202:1203-1206.

Brum G., and E. Rios. 1987. Intramembrane charge movement in frog skeletal muscle fibres. Properties of charge 2 [published erratum appears in (1988) *J. Physiol.* 396:581]. *J. Physiol.* 387:489-517.

Brum G., R. Fitts, G. Pizarro, and E. Rios. 1988. Voltage sensors of the frog skeletal muscle membrane require calcium to function in excitation-contraction coupling. *J. Physiol.* 398:475-505.

Pizarro G., R. Fitts, I. Uribe, and E. Rios. 1989. The voltage sensor of excitation-contraction coupling in skeletal muscle. Ion dependence and selectivity. *J. Gen. Physiol.* 94:405-428.

Ferreira G., J. Yi, E. Rios, and R. Shirokov. 1997. Ion-dependent inactivation of barium current through L-type calcium channels. *J. Gen. Physiol.* 109:449-461.

Isaev D., K. Solt, O. Gurtovaya, J.P. Reeves, and R. Shirokov. 2004. Modulation of the voltage sensor of L-type $Ca^{2+}$ channels by intracellular $Ca^{2+}$. *J. Gen. Physiol.* 123:555-571.

Kass R.S. 2004. Sodium Channel Inactivation Goes with the Flow. *J. Gen. Physiol.* 124:7-8.

Kiss L., J. LoTurco, and S.J. Korn. 1999. Contribution of the selectivity filter to inactivation in potassium channels. *Biophys. J.* 76:253–263.

Kuo C.C., W.Y. Chen, and Y.C. Yang. 2004. Block of tetrodotoxin-resistant $Na^+$ channel pore by multivalent cations: gating modi-fication and $Na^+$ flow dependence. *J. Gen. Physiol.* 124:27–42.

Lee A., S.T. Wong, D. Gallagher, B. Li, D.R. Storm, T. Scheuer, and W.A. Catterall. 1999. $Ca^{2+}$/calmodulin binds to and modulates P/Q-type calcium channels. *Nature* 399:155-159.

Lopez-Barneo J., T. Hoshi, S.H. Heinemann, and R.W. Aldrich. 1993. Effects of external cations and mutations in the pore region on C-type inactivation of Shaker potassium channels. *Receptors & Channels* 1:61-71.

Matveev V., R.S. Zucker, and A. Sherman. 2004. Facilitation through buffer saturation: constraints on endogenous buffering properties. *Biophys. J.* 86:2691-2709.

Noceti F., R. Olcese, N. Qin, J. Zhou, and E. Stefani. (1998). Effect of Bay K 8644(-) and the $\beta$2a subunit on $Ca^{2+}$-dependent inactivation in $\alpha$1C $Ca^{2+}$ channels. *J. Gen. Physiol.* 111:463-475.

Peterson B.Z., C.D. DeMaria, J.P. Adelman, and D.T. Yue. 1999. Calmodulin is the $Ca^{2+}$ sensor for $Ca^{2+}$-dependent inactivation of L-type calcium channels. *Neuron* 22:549-558.

Qin N., R. Olcese, M. Bransby, T. Lin, and L. Birnbaumer. 1999. $Ca^{2+}$-induced inhibition of the cardiac $Ca^{2+}$ channel depends on calmodulin. *Proc. Natl. Acad. Sci. USA* 96:2435-2438.

Sather W.A., and E.W. McCleskey. 2003. Permeation and selectivity of calcium channels. *Annu. Rev. Physiol.* 65:133-159.

Seifert R., E. Eismann, J. Ludwig, A. Baumann, and U.B. Kaupp. 1999. Molecular determinants of a $Ca^{2+}$-binding site in the pore of cyclic nucleotide-gated channels: S5/S6 segments control affinity of intrapore glutamates. *EMBO J.* 18:119–130.

Shirokov R., R. Levis, N. Shirokova, and E. Rios. 1992. Two classes of gating current from L-type Ca channels in guinea pig ventricular myocytes. *J. Gen. Physiol.* 99:863-895.

Starkus J.G., L. Kuschel, M.D. Rayner, and S.H. Heinemann. 1997. Ion conduction through C-type inactivated *Shaker* channels. *J. Gen. Physiol.* 110:539-550.

Starkus J.G., S.H. Heinemann, and M.D. Rayner. 2000. Voltage dependence of slow inactivation in *Shaker* potassium channels results from changes in relative $K^+$ and $Na^+$ permeabilities. *J. Gen. Physiol.* 115:107-122.

Talavera K., A. Janssens, N. Klugbauer, G. Droogmans, and B. Nilius. 2003. Pore structure influences gating properties of the T-type $Ca^{2+}$ channel $\alpha 1_G$. *J. Gen. Physiol.* 121:529–540.

Woodhull A.M. 1973. Ionic blockage of sodium channels in nerve. *J. Gen. Physiol.* 61:687–708.

Yatani A., A. Bahinski, M. Wakamori, S. Tang, Y. Mori, T. Kobayashi, and A. Schwartz. 1994. Alteration of channel characteristics by exchange of pore-forming regions between two structurally related $Ca^{2+}$ channels. *Mol. Cell. Biochem.* 140:93–102.

Zong Z.Q., J.Y. Zhou, and T. Tanabe. 1994. Molecular determinants of calcium-dependent inactivation in cardiac L-type calcium channels. *Biochem Biophys Res Commun.* 201(3):1117-11123.

Zuhlke R.D., G.S. Pitt, K. Deisseroth, R.W. Tsien, and H. Reuter. 1999. Calmodulin supports both inactivation and facilitation of L-type calcium channels. *Nature* 399:159-162.

**Acknowledgements**

The authors are grateful to John Reeves for valuable suggestions and discussions. The work was supported by NIH grants MH62838 to R.S. and NSF grant DMS-0417416 to V.M.

**FIGURE LEGENDS.**

**Figure 1.** Tail currents reveal that $Gd^{3+}$ reduces inactivation in $Ca^{2+}$.

(A) Voltage-pulse protocol used. 20 ms step to 200 mV was applied to relieve $Gd^{3+}$ block at different times of the pulse to 20 mV.

(B) Currents from a cell bathed in solution with 10 mM $Ca^{2+}$ and 0 $Gd^{3+}$. The peaks of tail currents in response to stepping from 200 to 20 mV followed the time course of inactivation. The dashed line through the peaks is the best fit by an exponential: $I = -I_0+\Delta I(1-e^{-kt})$ where $I_0$=979 pA, $\Delta$I=669 pA, and k=0.010 $ms^{-1}$. The ratio between the numbers of inactivated and non-inactivated channels after 500 ms at 20 mV can be estimated by: $\Delta I/(I_0-\Delta I)$. On average, it was 2.1 $\pm$ 0.17 (n= 6).

(C) Currents from the same cell bathed in solution with 10 mM $Ca^{2+}$ and 50 nM $Gd^{3+}$. The dashed line through the peaks is the best fit with $I_0$=986 pA, $\Delta$I=552 pA, and k=0.011 $ms^{-1}$. The averaged $\Delta I/(I_0-\Delta I)$ ratio was 1.24 $\pm$ 0.14 (n= 6).

(D) Currents from the same cell bathed in solution with 10 mM $Ca^{2+}$ and 1 $\mu$M $Gd^{3+}$. The dashed line through the peaks is the best fit with $I_0$=948 pA, $\Delta$I=328 pA, and k=0.007 $ms^{-1}$. The averaged $\Delta I/(I_0-\Delta I)$ ratio was 0.51 $\pm$ 0.13 (n= 6).

**Figure 2**. Inactivation of $Ba^{2+}$ currents in the presence of $Gd^{3+}$.

Currents were elicited similar to that in Fig 1. The 20 ms step to 200 mV was applied after 5 ms at 0 mV (traces *a* and *c*), or after 500 ms at 0 mV (traces *b* and *d*). Without the blocker (traces *a* and *b*), the peaks of the tails differ because of inactivation. With 25 nM $Gd^{3+}$ (traces *c* and *d*), currents elicited by the step from –90 to 0 mV were smaller

and decayed more rapidly. However, the 200 mV pulse after 5ms at 0 mV relieved the tonic $Gd^{3+}$ block to reveal the magnitude of the unblocked current (compare traces *a* and *c*). $Gd^{3+}$ did not change the magnitude of tail currents after 500 ms at 0 mV (compare traces *b* and *d*). The ratio between the numbers of inactivated and non-inactivated channels after 500 ms at 0 mV was estimated directly from the traces as indicated. On average, it was 0.43 $\pm$ 0.11 (n= 5) without $Gd^{3+}$ and 0.35 $\pm$ 0.09 after addition of 25 nM of $Gd^{3+}$.

**Figure 3**. The CAM1234 mutation of calmodulin reduced inactivation of $Ca^{2+}$ currents, but it did not alter open-channel block by $Gd^{3+}$. Currents were elicited by the same pulse protocol as in Fig. 1A. Only traces with 500 ms pulse from –90 to 20 mV are shown. Although in the absence of $Gd^{3+}$ (black traces) inactivation of currents at 20 mV was much less in the cell with CAM1234, application of 0.1 $\mu$M $Gd^{3+}$ (gray traces) reduced the peak and accelerated the decay of currents similarly in the wild type cell and in the cell with the mutated calmodulin. Since the step to 200 mV did not relieve inactivation (Fig. 1B), but relieved $Gd^{3+}$ block (see accompanying paper Babich et al., 2007), the ratio between the numbers of open and open-blocked channels after 500 ms at 20 mV can be simply estimated from the current before the step to 200 mV and from the peak of the tail current on the return from 200 to 20 mV, as indicated. On average, the ratio was 0.161 $\pm$ 0.012 in the wild type cells (n= 3 ) and 0.156 $\pm$ 0.014 (n= 4) in cells with CAM1234.

**Figure 4**. A model of ion-dependent inactivation.

**Figure 5**. Simulated $Ca^{2+}$ currents using the single-site approximation to calculate single-channel currents. The "inactivation-binding" coupling factor was $\gamma = 50$.

(A) Total currents. Voltage steps were from the holding potential –100 mV to -60 – 90 mV, increment 10 mV.

(B) Currents through inactivated channels.

(C) Peak current-voltage relationship.

(D) Rates of the best fits by the sum of an exponential and a constant to the decay phase of currents in the right-hand side of panel A.

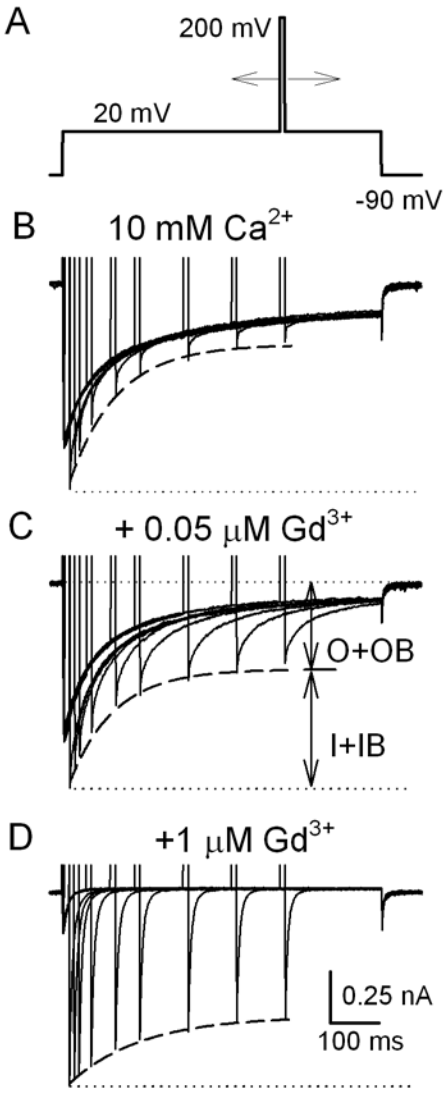
A
200 mV
20 mV
-90 mV
B
10 mM Ca2+
C
+ 0.05 μM Gd3+
O+OB
I+IB
D
+1 μM Gd3+
0.25 nA
100 ms

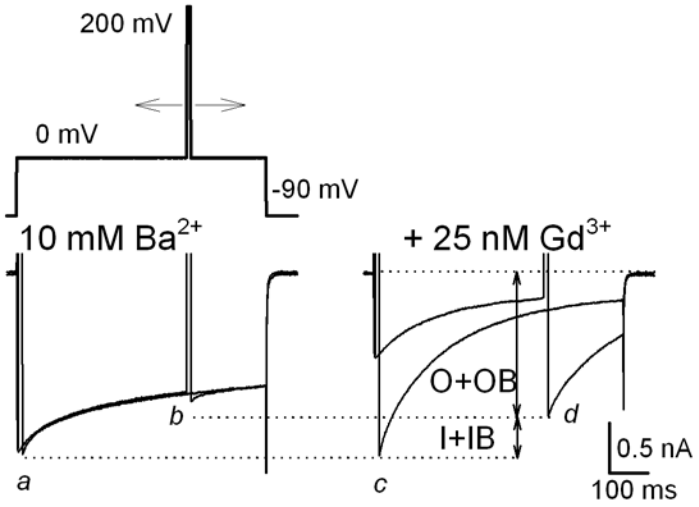
200 mV
0 mV
-90 mV
10 mM Ba2+
+ 25 nM Gd3+
O+OB
I+IB
b
d
a
c
0.5 nA
100 ms

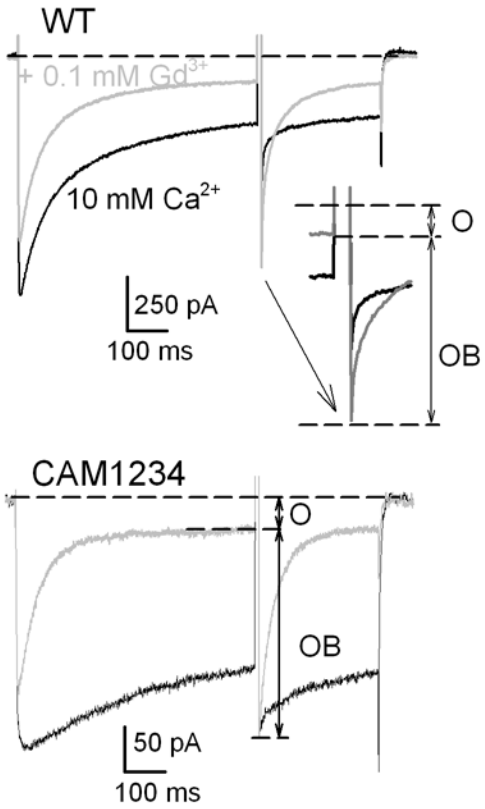
WT
+ 0.1 mM Gd3+
10 mM Ca2+
250 pA
100 ms
O
OB
CAM1234
O
OB
50 pA
100 ms

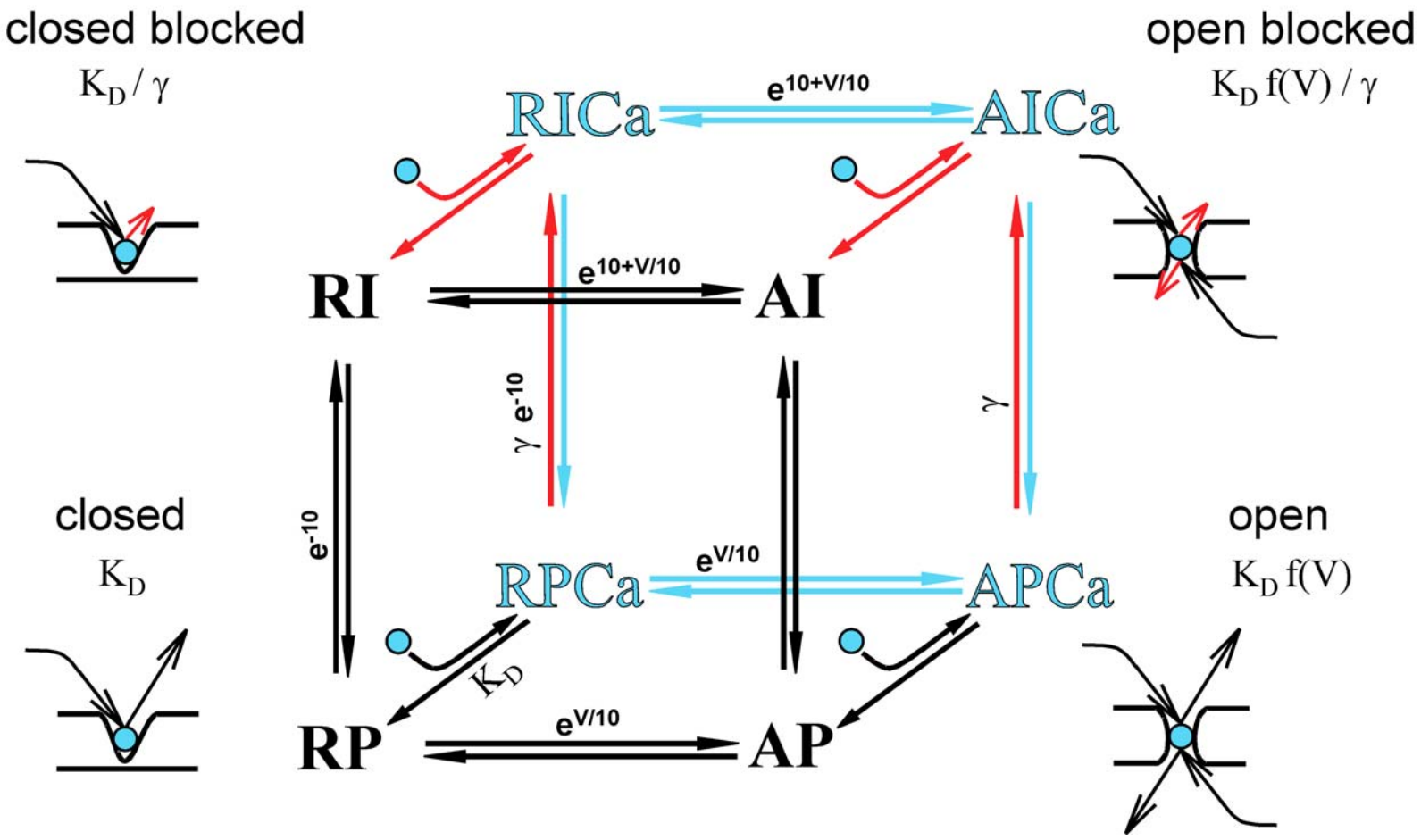
closed blocked
$K_D / \gamma$
open blocked
$K_D f(V) / \gamma$
RICa
$e^{10+V/10}$
AICa
RI
$e^{10+V/10}$
AI
$\gamma\ e^{-10}$
$\gamma$
$e^{-10}$
closed
$K_D$
open
$K_D f(V)$
RPCa
$e^{V/10}$
APCa
$K_D$
RP
$e^{V/10}$
AP

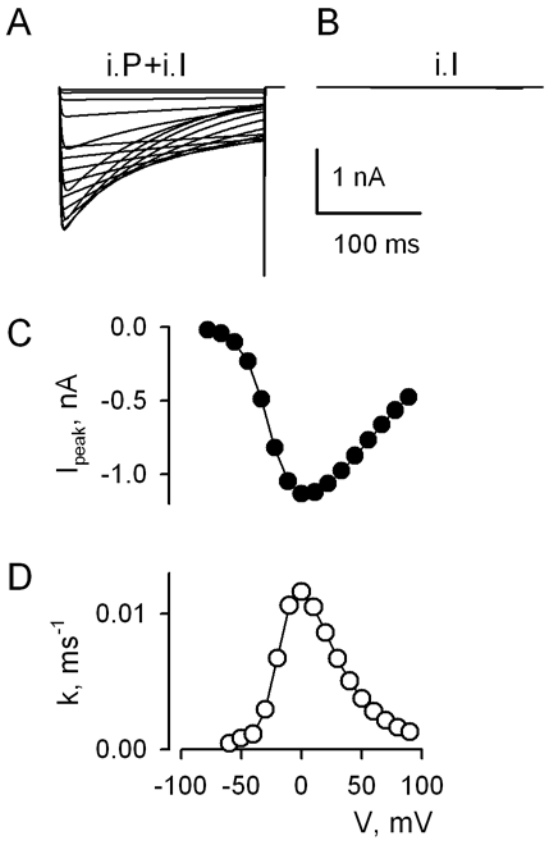
A
B
i.P+i.I
i.I
1 nA
100 ms
C
0.0
-0.5
-1.0
$I_{peak}$, nA
D
0.01
0.00
k, $ms^{-1}$
-100
-50
0
50
100
V, mV

**Supplemental figure 1S.**

Effect of series resistance (Rs) on simulated kinetics of inactivation. The simulations were done using script file cain.par. Typical experimental value for Rs is ≈10 MΩ, which includes resistance of the pipette and of the intracellular access to the membrane.

(A) Simulated ionic currents for Rs = 1 MΩ, γ=100.

(B) Simulated ionic currents for Rs = 20 MΩ, γ=100.

(C) Peak current-voltage relationships for currents in panels A and B

(D) Rates of the best fits by the sum of an exponential and a constant to the decay phase of currents in panels A and B.

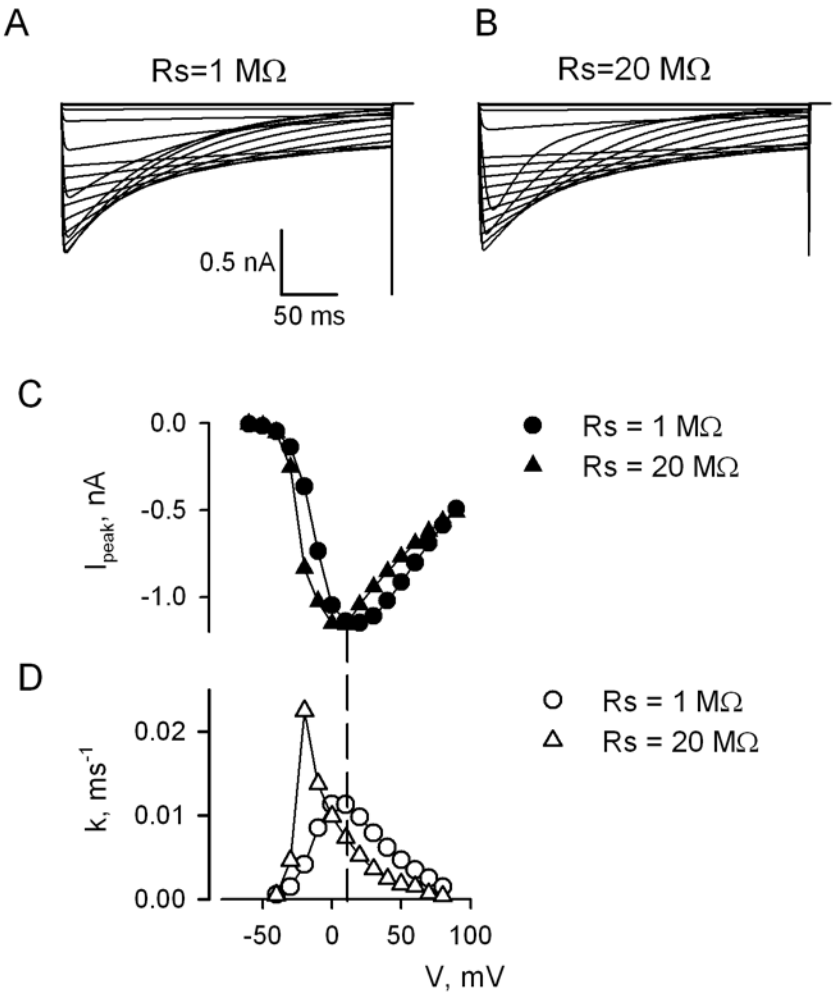
A
Rs=1 MΩ
0.5 nA
50 ms
B
Rs=20 MΩ
C
0.0
-0.5
-1.0
$I_{peak}$, nA
Rs = 1 MΩ
Rs = 20 MΩ
D
0.02
0.01
0.00
k, $ms^{-1}$
-50
0
50
100
V, mV
Rs = 1 MΩ
Rs = 20 MΩ

**Supplemental figure 2S.**

Effect of local $Ca^{2+}$ accumulation on simulated kinetics of inactivation. The simulations were done using script file cain2.par. Here, the inactivation-block coupling factor $\gamma$ in conducting states is a function of the single-channel current: $\gamma = \gamma_0 + \varepsilon\, i_{s.ch.}$. Rs was 5 MΩ throughout.

A) Simulated ionic currents for $\gamma_0$=50, $\varepsilon$=0.

(B) Simulated ionic currents for $\gamma_0$=50, $\varepsilon$=200.

(C) Peak current-voltage relationships for currents in panels A and B.

(D) Rates of the best fits by the sum of an exponential and a constant to the decay phase of currents in panels A and B.

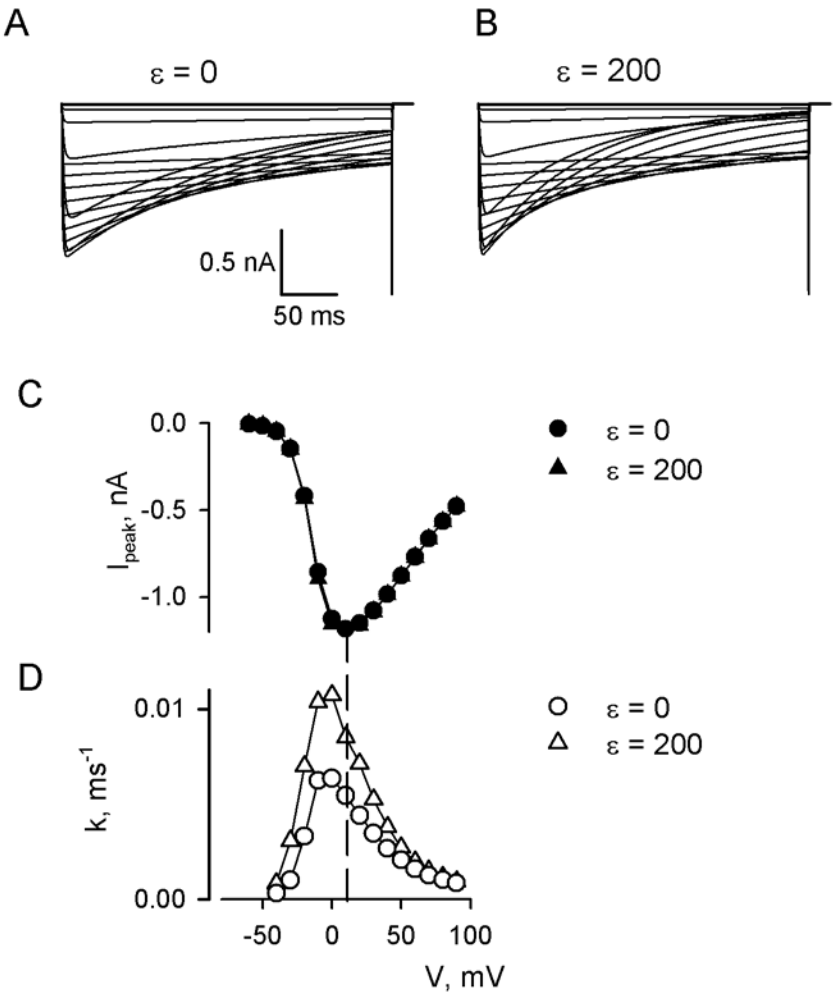
A
ε = 0
0.5 nA
50 ms
B
ε = 200
C
0.0
-0.5
-1.0
$I_{peak}$, nA
ε = 0
ε = 200
D
0.01
0.00
k, $ms^{-1}$
-50
0
50
100
V, mV
ε = 0
ε = 200

**Supplemental figure 3S.**

Simulation of inactivation in $Ba^{2+}$. For this, the “inactivation-binding” coupling factor in the script cain.par was $\gamma = 5$.

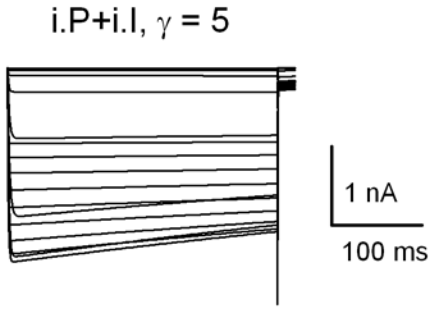
i.P+i.I, γ = 5
1 nA
100 ms